Research Article | Vol. 25, No. 23 | 13 Nov 2017 | OPTICS EXPRESS 28258
Optics EXPRESS

Periodically intensity-modulated pulses by optical parametric amplification for multicycle tunable terahertz pulse generation

GYÖRGY TÓTH,[1,2*] JÓZSEF A. FÜLÖP,[1,3,4] AND JÁNOS HEBLING[1,2,3]

[1]*MTA-PTE High-Field Terahertz Research Group, 7624 Pécs, Hungary*
[2]*Institute of Physics, University of Pécs, 7624 Pécs, Hungary*
[3]*Szentágothai Research Centre, University of Pécs, 7624 Pécs, Hungary*
[4]*ELI-ALP, ELI-Hu Nkft., 6720 Szeged, Hungary*
**tothgy@fizika.ttk.pte.hu*

Abstract: The superposition of signal and idler pulses in dual-chirped optical parametric amplification is proposed for the efficient generation of intensity-modulated pulses with periodic modulation. Both the duration and the modulation period are easily and independently adjustable. Numerical simulations for a three-stage optical parametric amplifier system predicted an efficiency as high as ~50% for about 40 mJ of output pulse energy at a wavelength of 2 μm. Sources of such intensity-modulated pulses near 1.6 μm or 2 μm wavelength, pumped by Ti:sapphire or Yb-doped lasers, can be ideally suited for intense multicycle THz pulse generation with tunable frequency and bandwidth by optical rectification for example in organic, semiconductor, or lithium niobate materials.

OCIS codes: (190.7110) Ultrafast nonlinear optics; (190.4970) Parametric oscillators and amplifiers; (320.5540) Pulse shaping.

References and links

1. M. C. Hoffmann and J. A. Fülöp, "Intense ultrashort terahertz pulses: generation and applications," J. Phys. D Appl. Phys. **44**, 083001 (2011).
2. H. Hirori, A. Doi, F. Blanchard, and K. Tanaka, "Single-cycle terahertz pulses with amplitudes exceeding 1 MV/cm generated by optical rectification in $LiNbO_3$," Appl. Phys. Lett. **98**, 091106 (2011).
3. C. Vicario, A. V. Ovchinnikov, S. I. Ashitkov, M. B. Agranat, V. E. Fortov, and C. P. Hauri, "Generation of 0.9-mJ THz pulses in DSTMS pumped by a Cr:Mg_2SiO_4 laser," Opt. Lett. **39**(23), 6632–6635 (2014).
4. J. A. Fülöp, Z. Ollmann, C. Lombosi, C. Skrobol, S. Klingebiel, L. Pálfalvi, F. Krausz, S. Karsch, and J. Hebling, "Efficient generation of THz pulses with 0.4 mJ energy," Opt. Express **22**(17), 20155–20163 (2014).
5. T. I. Oh, Y. J. Yoo, and Y. S. You, "andk K. Y. Kim, "Generation of strong terahertz fields exceeding 8 MV/cm at 1 kHz and real-time beam profiling," Appl. Phys. Lett. **105**, 041103 (2014).
6. M. Shalaby and C. P. Hauri, "Demonstration of a low-frequency three-dimensional terahertz bullet with extreme brightness," Nat. Commun. **6**, 5976 (2015).
7. D. Nicoletti and A. Cavalleri, "Nonlinear light-matter interaction at terahertz frequencies," Adv. Opt. Photonics **8**(3), 401–464 (2016).
8. L. J. Wong, A. Fallahi, and F. X. Kärtner, "Compact electron acceleration and bunch compression in THz waveguides," Opt. Express **21**(8), 9792–9806 (2013).
9. Z. Tibai, L. Pálfalvi, J. A. Fülöp, G. Almási, and J. Hebling, "THz-pulse-driven particle accelerators," in *4th EOS Topical Meeting on Terahertz Science & Technilogy* (Camogli, Italy, 2014).
10. E. A. Nanni, W. R. Huang, K.-H. Hong, K. Ravi, A. Fallahi, G. Moriena, R. J. D. Miller, and F. X. Kärtner, "Terahertz-driven linear electron acceleration," Nat. Commun. **6**, 8486 (2015).
11. L. Pálfalvi, J. A. Fülöp, Gy. Tóth, and J. Hebling, "Evanescent-wave proton postaccelerator driven by intense THz pulse," Phys. Rev. Spec. Top. Accel. Beams **17**, 031301 (2014).
12. A. Sharma, Z. Tibai, and J. Hebling, "Intense tera-hertz laser driven proton acceleration in plasmas," Phys. Plasmas **23**(6), 063111 (2016).
13. T. Plettner, P. P. Lu, and R. L. Byer, "Proposed few-optical cycle laser-driven particle accelerator structure," Phys. Rev. Spec. Top. Accel. Beams **9**, 111301 (2006).
14. A. S. Weling, B. B. Hu, N. M. Froberg, and D. H. Auston, "Generation of tunable narrow-band THz radiation from large aperture photoconducting antennas," Appl. Phys. Lett. **64**(2), 137–139 (1994).
15. T. Feurer, J. C. Vaughan, and K. A. Nelson, "Spatiotemporal Coherent Control of Lattice Vibrational Waves," Science **299**(5605), 374–377 (2003).

#303464 https://doi.org/10.1364/OE.25.028258
Journal © 2017 Received 27 Jul 2017; revised 5 Oct 2017; accepted 8 Oct 2017; published 31 Oct 2017

Optics EXPRESS

16. K.-L. Yeh, J. Hebling, M. C. Hoffmann, and K. A. Nelson, "Generation of high average power 1 kHz shaped THz pulses via optical rectification," Opt. Commun. **281**(13), 3567–3570 (2008).
17. Z. Chen, X. Zhou, C. A. Werley, and K. A. Nelson, "Generation of high power tunable multicycle terahertz pulses," Appl. Phys. Lett. **99**, 071102 (2011).
18. J. Lu, H. Y. Hwang, X. Li, S.-H. Lee, O.-P. Kwon, and K. A. Nelson, "Tunable multi-cycle THz generation in organic crystal HMQ-TMS," Opt. Express **23**(17), 22723–22729 (2015).
19. F. Ahr, S. W. Jolly, N. H. Matlis, S. Carbajo, T. Kroh, K. Ravi, D. N. Schimpf, J. Schulte, H. Ishizuki, T. Taira, A. R. Maier, and F. X. Kärtner, "Narrowband terahertz generation with chirped-and-delayed laser pulses in periodically poled lithium niobate," Opt. Lett. **42**(11), 2118–2121 (2017).
20. C. Vicario, M. Shalaby, F. Giorgianni, A. Ovchinnikov, O. Chefonov, and C. P. Hauri, "Broadband and narrowband terahertz source at extreme field strength," in Conference on Lasers and Electro-Optics, OSA Technical Digest (online) (Optical Society of America, 2017), paper Stu3J.6.
21. C. Vicario, A. V. Ovchinnikov, O. V. Chefonov, and C. P. Hauri, "Multi-octave spectrally tunable strong-field Terahertz laser," arXiv:1608.05319 (2016).
22. K. Wynne and J. J. Carey, "An integrated description of terahertz generation through optical rectification, charge transfer, and current surge," Opt. Commun. **256**(4–6), 400–413 (2005).
23. Y.-S. Lee, T. Meade, V. Perlin, H. Winful, and T. B. Norris, "Generation of narrow-band terahertz radiation via optical rectification of femtosecond pulses in periodically poled lithium niobate," Appl. Phys. Lett. **76**, 2505 (2000).
24. S. Carbajo, J. Schulte, X. Wu, K. Ravi, D. N. Schimpf, and F. X. Kärtner, "Efficient narrowband terahertz generation in cryogenically cooled periodically poled lithium niobate," Opt. Lett. **40**(24), 5762–5765 (2015).
25. K. Ravi, D. N. Schimpf, and F. X. Kärtner, "Pulse sequences for efficient multi-cycle terahertz generation in periodically poled lithium niobate," Opt. Express **24**(22), 25582–25607 (2016).
26. A. Stepanov, J. Hebling, and J. Kuhl, "Generation, tuning, and shaping of narrow-band, picosecond THz pulses by two-beam excitation," Opt. Express **12**(19), 4650–4658 (2004).
27. K.-H. Lin, C. A. Werley, and K. A. Nelson, "Generation of multicycle terahertz phonon-polariton waves in a planar waveguide by tilted optical pulse fronts," Appl. Phys. Lett. **95**, 103304 (2009).
28. G. Cirmi, M. Hemmer, K. Ravi, F. Reichert, L. E. Zapata, A.-L. Calendron, H. Cankaya, F. Ahr, O. D. Mücke, N. H. Matlis, and F. X. Kärtner, "Cascaded second-order processes for the efficient generation of narrowband terahertz radiation," J. Phys. At. Mol. Opt. Phys. **50**, 088002 (2017).
29. J. Hebling, G. Almási, I. Kozma, and J. Kuhl, "Velocity matching by pulse front tilting for large area THz-pulse generation," Opt. Express **10**(21), 1161–1166 (2002).
30. S.-W. Huang, E. Granados, W. R. Huang, K.-H. Hong, L. E. Zapata, and F. X. Kärtner, "High conversion efficiency, high energy terahertz pulses by optical rectification in cryogenically cooled lithium niobate," Opt. Lett. **38**(5), 796–798 (2013).
31. K. Ravi, W. R. Huang, S. Carbajo, X. Wu, and F. Kärtner, "Limitations to THz generation by optical rectification using tilted pulse fronts," Opt. Express **22**(17), 20239–20251 (2014).
32. Cs. Lombosi, Gy. Polónyi, M. Mechler, Z. Ollmann, J. Hebling, and J. A. Fülöp, "Nonlinear distortion of intense THz beams," New J. Phys. **17**, 083041 (2015).
33. K. L. Vodopyanov, "Terahertz-wave generation with periodically inverted gallium arsenide," Laser Phys. **19**(2), 305–321 (2009).
34. F. Blanchard, B. E. Schmidt, X. Ropagnol, N. Thiré, T. Ozaki, R. Morandotti, D. G. Cooke, and F. Légaré, "Terahertz pulse generation from bulk GaAs by a tilted-pulse-front excitation at 1.8 μm," Appl. Phys. Lett. **105**(24), 241106 (2014).
35. J. A. Fülöp, G. Polónyi, B. Monoszlai, G. Andriukaitis, T. Balciunas, A. Pugzlys, G. Arthur, A. Baltuska, and J. Hebling, "Highly efficient scalable monolithic semiconductor terahertz pulse source," Optica **3**(10), 1075–1078 (2016).
36. G. Polónyi, B. Monoszlai, G. Gäumann, E. J. Rohwer, G. Andriukaitis, T. Balciunas, A. Pugzlys, A. Baltuska, T. Feurer, J. Hebling, and J. A. Fülöp, "High-energy terahertz pulses from semiconductors pumped beyond the three-photon absorption edge," Opt. Express **24**(21), 23872–23882 (2016).
37. Gy. Polónyi, M. I. Mechler, J. Hebling, and J. A. Fülöp, "Prospects of Semiconductor Terahertz Pulse Sources," IEEE J. Sel. Top. Quantum Electron. **23**(4), 8501208 (2017).
38. P. Malevich, G. Andriukaitis, T. Flöry, A. J. Verhoef, A. Fernández, S. Ališauskas, A. Pugžlys, A. Baltuška, L. H. Tan, C. F. Chua, and P. B. Phua, "High energy and average power femtosecond laser for driving mid-infrared optical parametric amplifiers," Opt. Lett. **38**(15), 2746–2749 (2013).
39. H. Hoogland, A. Thai, D. Sánchez, S. L. Cousin, M. Hemmer, M. Engelbrecht, J. Biegert, and R. Holzwarth, "All-PM coherent 2.05 μm Thulium/Holmium fiber frequency comb source at 100 MHz with up to 0.5 W average power and pulse duration down to 135 fs," Opt. Express **21**(25), 31390–31394 (2013).
40. Q. Zhang, E. J. Takahashi, O. D. Mücke, P. Lu, and K. Midorikawa, "Dual-chirped optical parametric amplification for generating few hundred mJ infrared pulses," Opt. Express **19**(8), 7190–7212 (2011).
41. Z. Hong, Q. Zhang, P. Lan, and P. Lu, "Generation of few-cycle infrared pulses from a degenerate dual-pump OPCPA," Opt. Express **22**(5), 5544–5557 (2014).
42. Y. Yin, J. Li, X. Ren, Y. Wang, A. Chew, and Z. Chang, "High-energy two-cycle pulses at 3.2 μm by a broadband-pumped dual-chirped optical parametric amplification," Opt. Express **24**(22), 24989–24998 (2016).

Optics EXPRESS

43. Y. Fu, E. J. Takahashi, and K. Midorikawa, "Energy scaling of infrared femtosecond pulses by dual-chirped optical parametric amplification," IEEE Photonics J. **9**(3), 1503108 (2017).
44. Y. Yin, A. Chew, X. Ren, J. Li, Y. Wang, Y. Wu, and Z. Chang, "Towards Terawatt Sub-Cycle Long-Wave Infrared Pulses via Chirped Optical Parametric Amplification and Indirect Pulse Shaping," Sci. Rep. **8**, 45794 (2017).
45. E. Gaižaiskas, R. Grigonis, and V. Sirutkaitis, "Self- and cross-modulation effects in a synchronously pumped optical parametric oscillator," J. Opt. Soc. Am. B **19**(12), 2957–2966 (2002).
46. Gy. Tóth, L. Pálfalvi, L. Tokodi, J. Hebling, and J. A. Fülöp, "Scalable broadband OPCPA in Lithium Niobate with signal angular dispersion," Opt. Commun. **370**, 250–255 (2016).
47. G. New, *Introduction to Nonlinear Optics* (Cambridge University, 2011).
48. E. Kaksis, G. Almási, J. A. Fülöp, A. Pugžlys, A. Baltuška, and G. Andriukaitis, "110-mJ 225-fs cryogenically cooled Yb:CaF_2 multipass amplifier," Opt. Express **24**(25), 28915–28922 (2016).
49. Y. Deng, A. Schwarz, H. Fattahi, M. Ueffing, X. Gu, M. Ossiander, T. Metzger, V. Pervak, H. Ishizuki, T. Taira, T. Kobayashi, G. Marcus, F. Krausz, R. Kienberger, and N. Karpowicz, "Carrier-envelope-phase-stable, 1.2 mJ, 1.5 cycle laser pulses at 2.1 μm," Opt. Lett. **37**(23), 4973–4975 (2012).
50. A. Gaydardzhiev, I. Nikolov, I. Buchvarov, V. Petrov, and F. Noack, "Ultrabroadband operation of a femtosecond optical parametric generator based on BiB_3O_6 in the near-IR," Opt. Express **16**(4), 2363–2373 (2008).
51. N. Broeuf, D. Branning, I. Chaperot, E. Dauler, S. Guérin, G. Jaeger, A. Muller, and A. Migdall, "Calculating characteristics of noncollinear phase matching in uniaxial and biaxial crystals," Opt. Eng. **39**(4), 1016–1024 (2000).
52. D. E. Zelmon, D. L. Small, and D. Jundt, "Infrared corrected Sellmeier coefficients for congruently grown lithium niobate and 5 mol. % magnesium oxide-doped lithium niobate," J. Opt. Soc. Am. B **14**(12), 3319–3322 (1997).
53. N. Umemura, K. Yoshida, and K. Kato, "Phase-matching properties of $KNbO_3$ in the mid-infrared," Appl. Opt. **38**(6), 991–994 (1999).
54. D. A. Roberts, "Simplified Characterization of Uniaxial and Biaxial Nonlinear Optical Crystals: A Plea for Standardization of Nomenclature and Conventions," IEEE J. Quantum Electron. **28**(10), 2057–2074 (1992).
55. I. Shoji, T. Kondo, A. Kitamoto, M. Shirane, and R. Ito, "Absolute scale of second-order nonlinear-optical coefficients," J. Opt. Soc. Am. B **14**(9), 2268–2294 (1997).
56. R. DeSalvo, A. A. Said, D. J. Hagan, E. W. Van Stryland, and M. Sheik-Bahae, "Infrared to Ultraviolet Measurements of Two-Photon Absorption and n_2 in Wide Bandgap Solids," IEEE J. Quantum Electron. **32**(8), 1324–1333 (1996).
57. M. Sheik-Bahae and M. Ebrahimzadeh, "Measurements of nonlinear refraction in the second-order $\chi^{(2)}$ materials $KTiOPO_3$, $KNbO_3$, β-BaB_2O_4, and LiB_3O_5," Opt. Commun. **142**, 294–298 (1997).
58. O. E. Martinez, "Grating and prism compressors in the case of finite beam size," J. Opt. Soc. Am. B **3**(7), 929–934 (1986).
59. S. Backus, C. G. Durfee, M. M. Murnane, and H. C. Kapteyn, "High power ultrafast lasers," Rev. Sci. Instrum. **69**(3), 1207–1223 (1998).

1. Introduction

Intense, nearly single-cycle terahertz (THz) pulses can be efficiently generated by table-top sources [1–6]. Such pulses can be used in materials science [7] and for the acceleration of electrons [8–10] and protons [11, 12]. The waveguide and resonator structures proposed for electron acceleration can be more efficiently driven by multicycle THz pulses. Dielectric grating structures were proposed for laser-driven electron acceleration [13], where using multicycle THz pulses, rather than optical pulses, can be of significant advantage.

Various methods were proposed for multi-cycle or shaped THz pulse generation. Intensity-modulated laser pulses were used to drive photoconductive antennas [14] or optical rectification [15–21], where the THz waveform is determined by the intensity shape of the pump pulse [22]. Other approaches involved periodically poled generator crystals [23–25], transient polarization gratings [26], planar waveguides [27], or cascaded second-order processes [28].

Tilted-pulse-front pumping [29] of $LiNbO_3$ (LN) has been providing the highest THz pulse energies and efficiencies in the low-frequency part of the THz spectrum [4, 30], especially advantageous for particle acceleration, whereby limitations of this technology also became apparent [31, 32]. It was demonstrated recently that semiconductor nonlinear materials can provide an efficient alternative technology with scalability to highest THz pulse energies and field strengths [33–37]. These materials need to be pumped at an infrared wavelength sufficiently long to suppress two- and three-photon absorption [35, 36], ideally

Optics EXPRESS

delivered by efficient diode-pumped solid-state lasers [38, 39]. While rapidly developing, such laser sources cannot yet deliver pulses ideally suited to drive single- or multi-cycle THz pulse generation. Another, but generally less efficient possibility is to use and infrared optical parametric amplifier (OPA) as the pump source.

Here we propose an efficient method to generate high-energy periodically intensity-modulated pump pulses for multi-cycle THz pulse generation. The method is based on the interference of signal and idler pulses generated in an optical parametric amplifier (OPA). A high degree of flexibility in modulated pulse length and modulation frequency is achieved by using suitably chirped pump, signal, and idler pulses in a dual-chirped OPA (DC-OPA).

Previous studies of the DC-OPA concept were aiming at the generation of high-power ultrabroadband optical [40–44] or THz [43] pulses compressible to few-cycle pulse durations. Importantly, in all these cases either the signal or the idler pulses were used, rather than the superposition of both. In addition, the instantaneous frequency difference between the chirped signal and idler pulses was not constant. In contrast, our goal is to generate pulses with periodic intensity modulation by the superposition of signal and idler, which requires a constant instantaneous frequency difference between the chirped signal and idler pulses. Such periodically modulated pulses can be used to drive THz generation by optical rectification in organic, semiconductor, or lithium niobate materials.

This paper is organized as follows. In Section 2 conditions are formulated to produce the periodic intensity modulation by the superposition of the chirped signal and idler pulses. Section 3 describes the theoretical model used for numerical simulations. Section 4 presents the conceptual design study of a high-energy DC-OPA pump source. The conclusion is drawn in Section 5.

2. Periodically intensity-modulated pulses by DC-OPA

Multi-cycle THz pulses with constant carrier frequency can be generated by optical rectification using intensity-modulated optical pump pulses with a constant modulation period. Such a pump pulse can be generated by superposing two Fourier limited (FL) pulses with a frequency offset, for example the signal and idler pulses from an OPA (Fig. 1(a)). More flexibility can be achieved by using a pair of chirped pulses rather than FL pulses. Both the duration of the modulated pulse and the modulation period can be set by varying the chirp and the relative delay between the two pulses. As it will be shown below, in this case the signal and idler pulses from a suitably designed DC-OPA can be used (Fig. 1(b)).

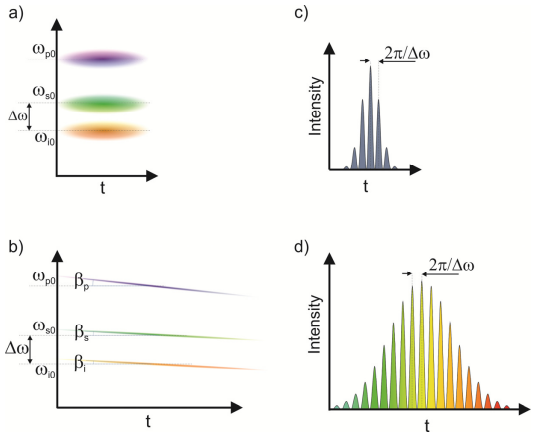

Fig. 1. Spectrograms of pump, signal, and idler pulses in case of FL (a) and chirped (b) pulses. The central frequencies of pump, signal, and idler are denoted by ω_{p0}, ω_{s0}, and ω_{i0}, respectively. (c) and (d) show the temporal intensities for the superstition of signal and idler.

Optics EXPRESS

2.1 Condition for periodic modulation

In parametric amplification energy conservation requires for the frequencies of pump (p), signal (s), and idler (i) that

$$\omega_{\mathrm{p}}(t)=\omega_{\mathrm{s}}(t)+\omega_{\mathrm{i}}(t) \tag{1}$$

holds. The superposition of signal and idler will have a constant intensity modulation period of $2\pi/\Delta\omega$ if

$$\Delta\omega=2\pi\cdot\Delta\nu=\omega_{\mathrm{s}}(t)-\omega_{\mathrm{i}}(t)=constant \tag{2}$$

holds. Our first goal is to determine the relation between the chirp of the pump and the signal under the condition of Eq. (2).

The electric field of a FL Gaussian pulse can be written as

$$E(t)=E_0 e^{-2\ln(2)\frac{t^2}{\Delta t^2}} e^{j\omega_0 t} \tag{3}$$

where E_0 is the amplitude of the electric field, Δt is the pulse duration at full width at half maximum (FWHM) of the intensity, ω_0 is the carrier angular frequency, and j is the imaginary unit. The corresponding amplitude spectrum is given by

$$\tilde{E}(\omega)=\mathcal{F}\{E(t)\}=\frac{1}{\sqrt{2\pi}}\int_{-\infty}^{\infty}E(t)e^{-j\omega t}\mathrm{d}t=\frac{E_0\Delta t}{\sqrt{\ln(2)}}e^{-\frac{\Delta t^2}{8\ln(2)}(\omega-\omega_0)^2} \tag{4}$$

After chirping and delaying the pulse, the electric field becomes

$$\begin{aligned}E(t)&=\frac{1}{\sqrt{2\pi}}\int_{-\infty}^{\infty}\tilde{E}(\omega)e^{-j\left(GD(\omega-\omega_0)+\frac{GDD}{2}(\omega-\omega_0)^2\right)}e^{j\omega t}\mathrm{d}\omega\\&=E_0\sqrt{\frac{\Delta t}{\tau}}e^{-2\ln(2)\frac{(t-GD)^2}{\tau^2}}e^{j\left[\omega_0 t+\beta(t-GD)^2-\frac{1}{2}\arctan\left(\frac{4\ln(2)GDD}{\Delta t^2}\right)\right]}\end{aligned} \tag{5}$$

where GD is the group delay, GDD is the group delay dispersion. Possible higher order dispersion terms were neglected here for the sake of simplicity. The duration of the chirped pulse (τ) and the chirp parameter (β, see also Fig. 1(b)) are given by

$$\tau=\Delta t\sqrt{1+\left(\frac{4\ln(2)\cdot GDD}{\Delta t^2}\right)^2}, \tag{6}$$

$$\beta=\left(2GDD+\frac{\Delta t^4}{8\ln^2(2)\cdot GDD}\right)^{-1}. \tag{7}$$

The instantaneous frequency can be calculated as

$$\omega(t)=\omega_0+2\beta(t-GD). \tag{8}$$

In the rest of the paper, quantities referring to the pump, signal, and idler pulses will be indexed by p, s, and i, respectively.

From the condition of periodic modulation, Eq. (2), with the help of Eqs. (1) and (8) one obtains for the relation between the chirp of the pump and the signal

Optics EXPRESS

$$\beta_s = \beta_p / 2. \tag{9}$$

As consequence, $\beta_i = \beta_s$. By substituting Eq. (7) for the chirp parameters in Eq. (9) and expressing GDD_s one obtains

$$GDD_s = GDD_p + \frac{\Delta t_p^4}{16\ln^2(2) GDD_p} + \sqrt{\left(GDD_p + \frac{\Delta t_p^4}{16\ln^2(2) GDD_p}\right)^2 - \frac{\Delta t_s^4}{4\ln^2(2)}}. \tag{10}$$

In case when the FL duration of the signal pulse is shorter or only slightly longer than that of the pump, the above expression simplifies to $GDD_s = 2GDD_p$.

2.2 Tuning the modulation period

The instantaneous frequencies of the interacting waves can be expressed from Eqs. (8), (9), and (1) in the following way:

$$\omega_p(t) = \omega_{p0} + 2\beta_p t, \tag{11a}$$

$$\omega_s(t) = \omega_{s0} + 2\beta_s(t - GD_{sp}) = \frac{\omega_{p0} + \Delta\omega_0}{2} + \beta_p(t - GD_{sp}), \tag{11b}$$

$$\omega_i(t) = \omega_p(t) - \omega_s(t) = \frac{\omega_{p0} - \Delta\omega_0}{2} + \beta_p(t + GD_{sp}). \tag{11c}$$

Here, $\Delta\omega_0/2$ is the deviation of the signal central frequency, ω_{s0}, from degeneracy and GD_{sp} is the group delay of the signal with respect to the pump. The frequency of intensity modulation for the superposition of signal and idler pulses can be obtained from Eqs. (2), (11b), and (11c) as

$$\Delta\omega = \omega_s(t) - \omega_i(t) = \Delta\omega_0 - 2\beta_p \cdot GD_{sp}. \tag{12}$$

Obviously, the intensity modulation frequency is determined by the offset of the signal central frequency from degeneracy, the chirp of the pump, and the temporal delay between the (chirped) pump and the (chirped) signal seed. An easy way of tuning the modulation frequency is to change the group delay GD_{sp}. An approximate limit on the tuneability is set by $|GD_{sp}| \lesssim (\tau_s - \tau_p)/2$ due to the finite pulse durations and the reduction of the OPA efficiency for large pump-signal delays. Equation (12) can be cast into a more practical form by using Eqs. (6) and (7):

$$\Delta\omega = \Delta\omega_0 - \frac{4\ln(2)\sqrt{N^2 - 1}}{\Delta t_p^2 N^2} \cdot GD_{sp}, \tag{13}$$

where $N = \tau_p / \Delta t_p$ gives the stretching factor for the pump.

In practical situations, a jitter between the pump and the signal pulses can result in a fluctuation of the modulation frequency. Figure 2 shows the calculated relative deviation in the intensity modulation frequency caused by a 40-fs jitter between pump and signal as function of the FL pump pulse duration and the pump stretching factor. The jitter-free ($GD_{sp} = 0$) modulation frequency was $\Delta\omega_0/2\pi = 1\,\mathrm{THz}$. For a given FL pump pulse duration, a sufficiently large stretching factor can reduce the modulation frequency

Optics EXPRESS

fluctuation below any desired limit. For example, in case of 200-fs FL pump pulses, a stretching factor of about 40 will limit the modulation frequency fluctuation below 1%.

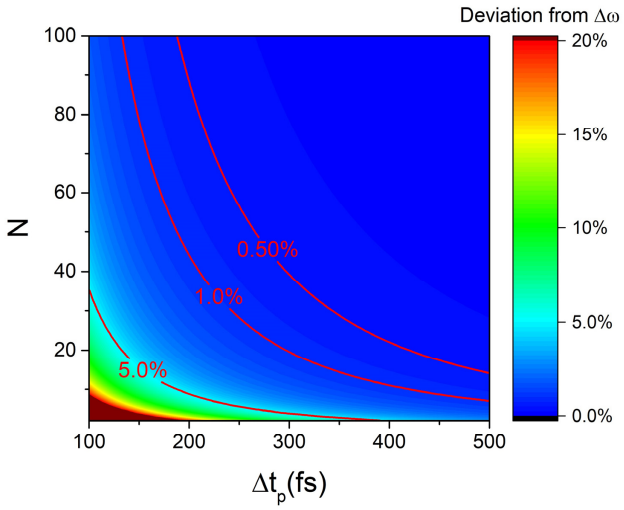

Fig. 2. Relative deviation in the intensity modulation frequency caused by a 40-fs jitter between pump and signal as function of the FL pump pulse duration and the pump stretching factor. The jitter-free modulation frequency was 1 THz.

2.3 Stretched pulse durations

In a typical practical situation, the FL pump pulse duration is given by the available pump laser. The necessary $N = \tau_p / \Delta t_p$ pump stretching factor can be determined by the desired length of the modulated pulse. The condition for the constant intensity modulation period can be used to determine the necessary signal stretching factor. To this end, Eq. (9) can be written in a more useful form with the help of Eqs. (6) and (10):

$$M = \frac{\tau_s}{\tau_p} = \frac{\mu}{N}\sqrt{1+\frac{\left(N^2+\sqrt{N^4-4\mu^4\left(N^2-1\right)}\right)^2}{\mu^4\left(N^2-1\right)}}. \qquad (14)$$

The derivation of this formula is outlined in the Appendix. Here, $\mu = \Delta t_s / \Delta t_p$ is the ratio of the signal and pump FL pulse durations.

Figure 3 shows the stretched pulse duration ratio M as function of the pump stretching factor N and the ratio μ of the FL pulse durations. For an efficient use of the pump energy the stretched signal duration should be approximately equal or larger than the stretched pump ($M \geq 1$), which holds if $\mu \lesssim 2$. On the other hand, a much too long signal ($M \gg 1$, corresponding to $\mu \lesssim 0.25$) would result in the inefficient use of the input signal energy. Therefore, a choice of $0.25 \lesssim \mu \lesssim 2$ is best. In this range, the pump stretching factor N can be freely varied while M remains nearly unchanged (Fig. 3), allowing for a large flexibility in the length of the modulated pulse. In addition, within this range, smaller μ values (with larger M) ensure good tunability of the intensity modulation period (without a significant reduction of the OPA efficiency, see Section 3.2).

Optics EXPRESS

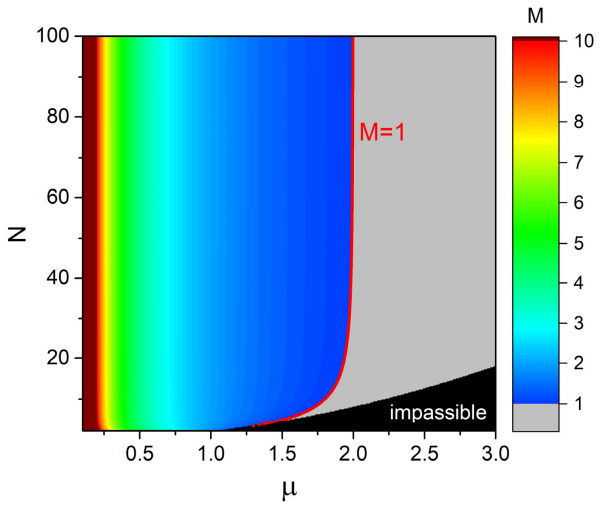

Fig. 3. The stretched pulse duration ratio M as function of the pump stretching factor N and the ratio $\mu = \Delta t_s / \Delta t_p$ of the FL pulse durations.

3. Theoretical model for simulations

In order to investigate the feasibility of our concept for the generation of intensity modulated pulses with a constant modulation period and to present a practical design study of a multi-stage OPA system we carried out numerical simulations. The coupled wave equations in the slowly varying envelope approximation were numerically solved. The time-dependent electric field is given by

$$E(\mathbf{r},t) = \frac{1}{2}\sum_{l=\mathrm{p,s,i}} A_l(\mathbf{r},t)\, e^{j(\mathbf{k}_l\mathbf{r}-\omega_l t)} + c.c., \tag{15}$$

where A_l is the slowly varying complex amplitude, $\mathbf{k}_l$ is the wave vector, and $l = \mathrm{p, s, i}$ for the pump, signal, and idler, respectively. The one-dimensional coupled wave equations in the following form were numerically solved [45, 46]:

$$\begin{aligned}\frac{\partial}{\partial z}A_\mathrm{p}(\omega,z,\rho) &= j\left(\mathbf{k}_\mathrm{p}(\omega)\mathbf{e}_z - \frac{\omega}{v_\mathrm{s}}\right)A_\mathrm{p}(\omega,z,\rho)\\ &+ j\frac{\omega_\mathrm{p} d_{eff}}{n_\mathrm{p} c}\mathcal{F}\left\{A_\mathrm{s}(\tau,z,\rho)\,A_\mathrm{i}(\tau,z,\rho)\,e^{j\Delta\mathbf{k}e_z z}\right\}\\ &+ j\frac{\omega_\mathrm{p}\varepsilon_0 n_2 n_\mathrm{p}}{2}\mathcal{F}\left\{A_\mathrm{p}(\tau,z,\rho)\left(2\left|A_\mathrm{s}(\tau,z,\rho)\right|^2 + 2\left|A_\mathrm{i}(\tau,z,\rho)\right|^2 + \left|A_\mathrm{p}(\tau,z,\rho)\right|^2\right)\right\},\end{aligned} \tag{16a}$$

$$\begin{aligned}\frac{\partial}{\partial z}A_\mathrm{s}(\omega,z,\rho) &= j\left(\mathbf{k}_\mathrm{s}(\omega)\mathbf{e}_z - \frac{\omega}{v_\mathrm{s}}\right)A_\mathrm{s}(\omega,z,\rho)\\ &+ j\frac{\omega_\mathrm{s} d_{eff}}{n_\mathrm{s} c}\mathcal{F}\left\{A_\mathrm{p}(\tau,z,\rho)\,A_\mathrm{i}^*(\tau,z,\rho)\,e^{-j\Delta\mathbf{k}e_z z}\right\}\\ &+ j\frac{\omega_\mathrm{s}\varepsilon_0 n_2 n_\mathrm{s}}{2}\mathcal{F}\left\{A_\mathrm{s}(\tau,z,\rho)\left(\left|A_\mathrm{s}(\tau,z,\rho)\right|^2 + 2\left|A_\mathrm{i}(\tau,z,\rho)\right|^2 + 2\left|A_\mathrm{p}(\tau,z,\rho)\right|^2\right)\right\},\end{aligned} \tag{16b}$$

Optics EXPRESS

$$\frac{\partial}{\partial z}A_{\mathrm{i}}(\omega,z,\rho)=j\left(\mathbf{k}_{\mathrm{i}}(\omega)\mathbf{e}_z-\frac{\omega}{v_{\mathrm{s}}}\right)A_{\mathrm{i}}(\omega,z,\rho)$$
$$+j\frac{\omega_{\mathrm{i}}d_{eff}}{n_{\mathrm{i}}c}\mathcal{F}\left\{A_{\mathrm{p}}(\tau,z,\rho)A_{\mathrm{s}}^{*}(\tau,z,\rho)e^{-j\Delta\mathbf{k}\mathbf{e}_z z}\right\}$$
$$+j\frac{\omega_{\mathrm{i}}\varepsilon_0 n_2 n_i}{2}\mathcal{F}\left\{A_{\mathrm{i}}(\tau,z,\rho)\left(2\left|A_{\mathrm{s}}(\tau,z,\rho)\right|^2+\left|A_{\mathrm{i}}(\tau,z,\rho)\right|^2+2\left|A_{\mathrm{p}}(\tau,z,\rho)\right|^2\right)\right\}. \quad (16c)$$

In these equations, each first term on the right-hand side describes the effect of material dispersion in the signal-pulse moving frame. The second terms describe optical parametric amplification. The third terms describe self- and cross-phase modulation. Here, ρ is the radial cylindrical coordinate. The diffraction was neglected, and the differential equation system was solved for different values of ρ, thereby enabling to take into account radial intensity variations. The unit vector along the *z*-axis (the signal propagation direction) is denoted by $\mathbf{e}_z$, the signal group velocity by v_s, the effective nonlinear coefficient by $d_{\mathrm{eff}}=\chi^{(2)}_{\mathrm{eff}}/2$, the speed of light by c, the wave-vector mismatch by $\Delta\mathbf{k}=\mathbf{k}_{\mathbf{p}}-\mathbf{k}_{\mathbf{s}}-\mathbf{k}_{\mathbf{i}}$, the vacuum permittivity by ε_0, and the nonlinear refractive index by $n_2=3\chi^{(3)}/4n^2c\varepsilon_0$ [47]. In the signal-pulse moving frame $\tau=t-z/v_s$ holds. At the input, the pump was assumed to have a super-Gaussian intensity profile and the signal was Gaussian:

$$A_{\mathrm{s}}(t,z=0,\rho)=\frac{4\ln^{\frac{3}{4}}(2)}{\sqrt{\varepsilon_0 c n_{\mathrm{s}}\pi^{\frac{3}{2}}\Delta t_{\mathrm{s}}\,w_{\mathrm{s}}}}\sqrt{W_{\mathrm{s}}}e^{-2\ln(2)\frac{t^2}{\Delta t_{\mathrm{s}}^2}}e^{-2\ln(2)\frac{\rho^2}{w_{\mathrm{s}}^2}}, \quad (17a)$$

$$A_{\mathrm{p}}(t,z=0,\rho)=\frac{4\sqrt{2\ln(2)}}{\sqrt{\varepsilon_0 c n_{\mathrm{p}}\Delta t_{\mathrm{p}}\pi w_{\mathrm{p}}}}\sqrt{W_{\mathrm{p}}}e^{-2\ln(2)\frac{t^2}{\Delta t_{\mathrm{p}}^2}}e^{-8\ln(2)\frac{\rho^4}{w_{\mathrm{p}}^4}}. \quad (17b)$$

Here, $w_{s,p}$ is the full-width beam diameter at half-maximum (FWHM) of the intensity and $W_{s,p}$ is the initial pulse energy.

4. Conceptual design study

The suitability of the concept for the generation of intensity modulated pulses with a constant modulation period was investigated by numerical simulations. As an example, here we present the feasibility study for the multi-stage OPA system shown in Fig. 4, designed for driving multi-cycle THz sources. Pump pulses of 80 mJ energy, 200 fs FL pulse duration were assumed, delivered by an Yb:CaF_2 laser system operating at 1.03 µm central wavelength [48]. Seed pulses of 5 nJ energy, 125 fs FL pulse duration, and 2.06 µm central wavelength can be delivered by a synchronized Tm,Ho-doped laser amplifier [39]. The signal is preamplified to the sub-mJ level in two subsequent noncollinear OPA stages, pumped by a small fraction of the available pump energy. The noncollinear phase matching geometry enables an easy separation of the signal from the pump and idler beams. The major portion of the pump energy is used to pump the DC-OPA stage. The pump pulses are stretched according to the desired length of the intensity-modulated output pulse. The preamplified signal pulses are stretched according to Eq. (14) and amplified in the collinear DC-OPA stage. The superposition of signal and idler generates the desired intensity modulated pulses with constant period. These pulses are separated from the pump by a dichroic mirror or by a polarizing filter. We note that a similar concept can be applied to a pump wavelength of 0.8

Optics EXPRESS

µm, delivered by a Ti:sapphire laser. In this case intensity-modulated pulses near 1.6 µm could be generated, ideally suited to drive organic-crystal based THz sources.

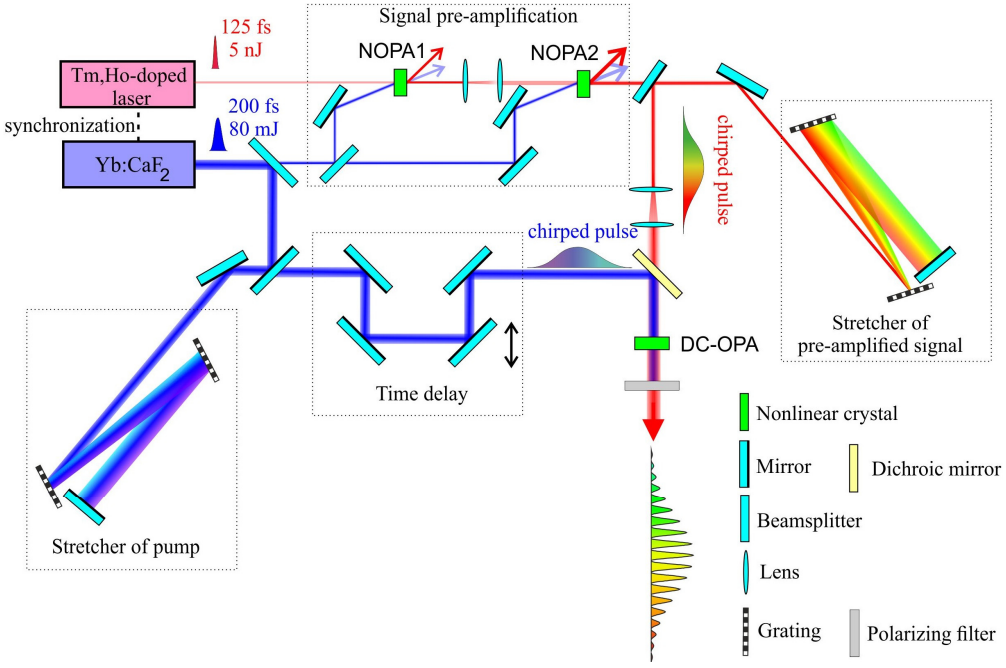

Fig. 4. Schematics of the simulated DC-OPA setup.

4.1 Selection of the nonlinear crystals

For multi-cycle THz pulse generation the frequency of intensity modulation should be equal to the desired THz frequency. As this is much smaller than the optical frequencies, a nearly-degenerate OPA should be used. Ultrabroadband amplification was demonstrated in a 1-µm pumped degenerate OPA using $LiNbO_3$ (LN) crystals [49]. An even larger bandwidth can be expected in $KNbO_3$ (KN) [50]. Figure 5 shows the calculated phase mismatch as function of the signal wavelength for LN and KN with 5 mm thickness, both for collinear as well as noncollinear phase matching geometries, in the latter case for $\alpha = 0.5°$ internal pump-signal noncollinearity angles. (Phase matching was set to 2.074 µm wavelength, corresponding to a 1 THz intensity modulation frequency.) In all cases excellent phase matching can be achieved over the laser bandwidth (shaded range in Fig. 5).

Optics EXPRESS

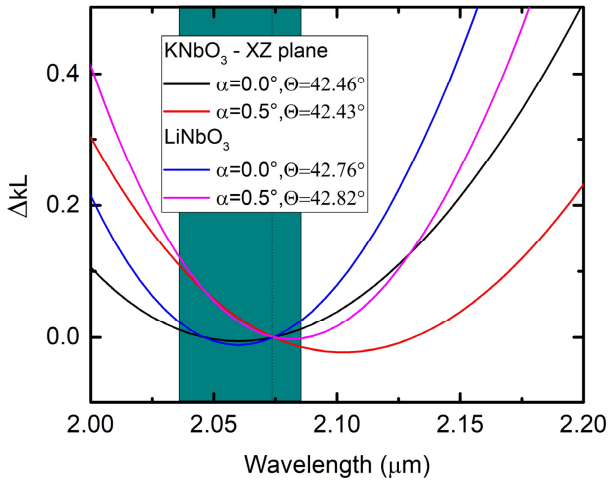

Fig. 5. Phase mismatch as function of the signal wavelength in LN and KN for collinear ($\alpha = 0°$) and noncollinear ($\alpha = 0.5^{\circ}$) geometries. The shaded range indicates the bandwidth of the seed laser.

The wave vector mismatch was approximated by its projection onto the pump propagation direction [51]. Refractive index data were taken from Refs [52]. and [53] for LN and KN, respectively. In all cases the signal and idler had parallel polarizations, perpendicular to that of the pump, enabling to use a polarization filter (beamsplitter) at the DC-OPA output.

Both LN and KN have a large effective nonlinear coefficient. In case of LN $d_{\text{eff}} = d_{31}\sin(\theta) - d_{22}\cos(\theta) = 4.5\ \text{pm/V}$ [54]. Here, θ is the angle between the propagation direction of pump and the optic axis of the crystal. In case of KN $d_{\text{eff}} = d_{31}\sin(\theta) = 6\ \text{pm/V}$ [55]. Here, θ is the angle between the propagation direction of the pump and the Z axis of crystal in the XZ plane. The values of $n_2 = 0.91\times10^{-15}\ \text{cm}^2/\text{W}$ [56] and $n_2 = 1.87\times10^{-15}\ \text{cm}^2/\text{W}$ [57] were used for the nonlinear refractive index of LN and KN, respectively. In the investigated cases related self- and cross-phase modulation effects were not significant.

In the numerical simulations discussed below LN was chosen as the nonlinear crystal for all OPA stages, including the DC-OPA.

4.2 Simulation results

Numerical simulations were carried out for the setup shown in Fig. 4 using the model described in Section 3. We note that all losses from the stretcher and the Fresnel losses were neglected in this calculation. The losses in the stretcher depend on the grating type. Typically, for a reflection-grating stretcher, these are about 30%, and for a transmission-grating stretcher less than 10%. The Fresnel losses can be reduced below 1%.

As mentioned above, the FL pulse duration was 200 fs at 1.03 μm central wavelength for the pump and 125 fs at 2.06 μm central wavelength for the signal seed. The subsequent OPA stages were pumped by 50 μJ, 5 mJ, and 75 mJ energy. The most important input and output parameters of the two noncollinear preamplifier stages are listed in Table 1. The angle between the propagation directions of pump and signal was $\alpha = 0.5°$ inside the LN crystal and the angle between the optic axis of the crystal and the propagation direction of the pump was $\theta = 42.82°$. The signal output of the first stage was used as input for the second stage. We note that central frequency of the signal is not changing during the nonlinear interaction process because of the excellent phase matching.

Optics EXPRESS

Table 1. Parameters of the two noncollinear OPA preamplifier stages. W_p: input pump energy, W_{s0}: input signal energy, $w_{s,p}$: FWHM beam diameter of signal (s) and pump (p), L: length of the LN nonlinear crystal, W_s: output amplified signal pulse energy.

Stage	W_p	W_{s0}	$w_{s,p}$	L	W_s
1st stage	50 μJ	5 nJ	0.8 mm	2.4 mm	6.3 μJ
2nd stage	5 mJ	6.3 μJ	8 mm	1.5 mm	0.53 mJ

Prior to entering the third, DC-OPA stage both the signal and the pump pulses were stretched by grating stretchers (Fig. 4). Both the GDD as well as the 3rd-order dispersion were taken into account [58, 59]. For the pump, a pair of 600-lines/mm gratings was assumed. The angle of incidence was $\gamma = 23°$, deviating from the Littrow configuration by only 5°. As mentioned in Section 3.3, the pump stretching factor can be determined by the desired length of the modulated pulse. In the simulations, 5 ps and 10 ps were considered (Table 2).

For given FL pulse durations, once the pump stretching factor has been chosen as desired, the required signal stretching factor and the corresponding GDD can be determined from Eqs. (14) and (10), respectively. For our case of $\mu = \Delta t_s / \Delta t_p = 0.625$, and the 5-ps and 10-ps stretched pump pulses, Eq. (14) gives a stretched signal duration of 16 ps and 32 ps, respectively (Table 2). As the FL signal pulse duration is shorter than that of the pump, $GDD_s = 2GDD_p$ holds to a good approximation (see Section 3.1). This relation can be easily fulfilled by using a grating pair with identical geometry but with 300-lines/mm rule density for the signal (i.e. $d_s = 2d_p$ in terms of the grating pitch), as obvious from the expression of the GDD for a grating pair [55],

$$GDD\left(\lambda, d, \gamma, L_f\right) = \frac{\lambda^3 L_g}{\pi c^2 d^2}\left(1 - \left(\frac{\lambda}{d} - \sin\gamma\right)^2\right)^{-3/2}, \tag{18}$$

where L_g is the distance between the grating surfaces. Due to the broadband phase matching a flexible tuning of the intensity modulation period is possible by changing the pump-signal delay, GD_{sp}, according to Eq. (13) where $\Delta\omega_0 = 0$ holds.

Table 2. Parameters of the DC-OPA. η: efficiency of the DC-OPA stage, η_Σ efficiency of the entire system including also the two preamplifier stages, W_{s+i}: energy of the intensity-modulated output pulse (superposition of signal and idler).

$\Delta\nu$ (THz)	1	1	0.5
τ_p (ps)	5	10	10
τ_s (ps)	16	32	32
GD_{sp} (ps)	2.27	4.53	2.27
w_p (mm)	5.2	4.8	4.8
w_s (mm)	8	8	8
L (mm)	1.7	2.3	2.3
L_g (cm)	23.9	47.9	47.9
η (%)	52.1	52.3	52.3
η_Σ (%)	48.9	49	49
W_{s+i} (mJ)	39.1	39.2	39.2

The results of the simulations are summarized in Table 2 and Fig. 6. Three representative cases were simulated to demonstrate the feasibility and flexibility of the scheme: 1 THz modulation frequency with 5 ps and 10 ps pulse durations, and 0.5 THz modulation frequency

Optics EXPRESS

with 10 ps pulse duration. The calculated pulse forms support the expectation that high-quality shaped pulses can be generated by the proposed DC-OPA method with a highly uniform intensity modulation frequency. For a given pump laser the setup can be flexibly configured to deliver a broad range of pulse lengths and modulation frequencies, which can be tailored to the need of different applications. We note that saturation in the DC-OPA can result in a flat-top modulated pulse, as can be seen in Fig. 6(b). Furthermore, according to Fig. 2, a temporal jitter of 20 fs between the pump and the signal results in a very small fluctuation of the modulation frequency of less than 1% in all investigated cases ensuring highly stable pulse forms.

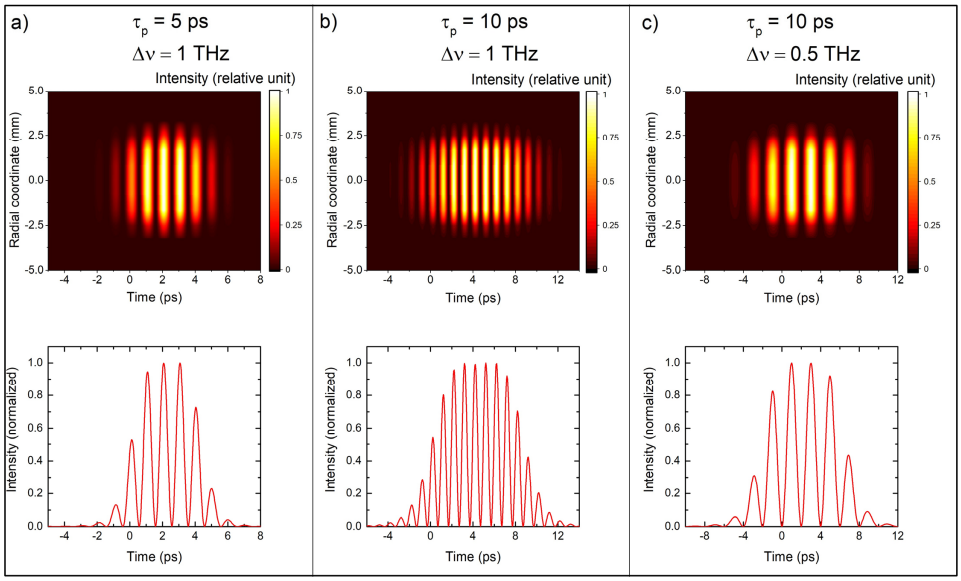

Fig. 6. Temporal and spatial intensity profiles of intensity-modulated pulses obtained by the superposition of signal and idler pulses in the DC-OPA for 5-ps pump pulses and 1 THz modulation frequency (a), 10-ps pump pulses and 1 THz modulation frequency (b), and 10-ps pump pulses and 0.5 THz modulation frequency (c). The lower panels show the temporal intensity shapes at the beam center.

In all cases a conversion efficiency of about 52% was predicted in the DC-OPA stage, and about 49% for the entire system including also the two preamplifier stages. Such uniquely high efficiencies are the result of utilizing both the signal and idler pulses from the DC-OPA. According to Table 2, the efficiency is essentially independent of tuning the modulation frequency. This holds as long as the desired modulation frequency remains much smaller than the bandwidth of the signal pulse (in other words, the pump-signal delay remains much smaller than the stretched signal duration).

5. Conclusion

Utilizing both signal and idler pulses in OPA for the generation of intensity-modulated pulses was proposed. A constant intensity modulation period was achieved by using chirped pump and signal pulses (dual-chirped OPA) for which design conditions were given by simple analytical expressions. Easy tunability of the modulation frequency is enabled by introducing a time delay between the pump and the signal pulses. A conceptual design study was presented for a complete three-stage OPA system. The numerical simulations predicted an efficiency as high as ~50% for about 40 mJ output pulse energy at a wavelength of 2 µm. Such flexibly shapeable pulse sources, operating near 1.6 µm or 2 µm and pumped by compact Ti:sapphire or Yb-doped lasers, can be ideally suited to drive organic or

Optics EXPRESS

semiconductor THz sources. These can deliver intense multi-cycle THz pulses with tunable frequency, enabling new applications in materials science and the construction of compact particle accelerators.

Appendix

We would like to calculate $M = \frac{\tau_s}{\tau_p}$. According to Eq. (6),

$$\tau_s = \Delta t_s \sqrt{1 + \left(\frac{4\ln(2) \cdot GDD_s}{\Delta t_s^{\,2}} \right)^2} \tag{19}$$

and

$$\tau_p = \Delta t_p \sqrt{1 + \left(\frac{4\ln(2) \cdot GDD_p}{\Delta t_p^{\,2}} \right)^2} = \Delta t_p \cdot N. \tag{20}$$

It follows:

$$GDD_p = \frac{\Delta t_p^2 \sqrt{N^2 - 1}}{4\ln(2)}. \tag{21}$$

By substituting Eq. (10) into Eq. (19) and using Eq. (21) one obtains:

$$\tau_s = \Delta t_s \sqrt{1 + \left(\frac{4\ln(2) \cdot \left[GDD_p + \frac{\Delta t_p^4}{16\ln^2(2) GDD_p} + \sqrt{\left(GDD_p + \frac{\Delta t_p^4}{16\ln^2(2) GDD_p} \right)^2 - \frac{\Delta t_s^4}{4\ln^2(2)}} \right]}{\Delta t_s^{\,2}} \right)^2} =$$

$$\Delta t_s \sqrt{1 + \left(\frac{4\ln(2) \cdot \left[\frac{\Delta t_p^2 \sqrt{N^2 - 1}}{4\ln(2)} + \frac{\Delta t_p^2}{4\ln(2)\sqrt{N^2 - 1}} + \sqrt{\left(\frac{\Delta t_p^2 \sqrt{N^2 - 1}}{4\ln(2)} + \frac{\Delta t_p^2}{4\ln(2)\sqrt{N^2 - 1}} \right)^2 - \frac{\Delta t_s^4}{4\ln^2(2)}} \right]}{\Delta t_s^{\,2}} \right)^2} =$$

$$\Delta t_s \sqrt{1 + \left(\left(\frac{\Delta t_p}{\Delta t_s} \right)^2 \sqrt{N^2 - 1} + \left(\frac{\Delta t_p}{\Delta t_s} \right)^2 \frac{1}{\sqrt{N^2 - 1}} + \sqrt{\left(\frac{\Delta t_p}{\Delta t_s} \right)^4 \left(\sqrt{N^2 - 1} + \frac{1}{\sqrt{N^2 - 1}} \right)^2 - 4} \right)^2}. \tag{22}$$

With the notation $\mu = \frac{\Delta t_s}{\Delta t_p}$, Eq. (22) becomes:

Optics EXPRESS

$$\tau_s = \Delta t_s \sqrt{1+\left(\left(\frac{1}{\mu}\right)^2\sqrt{N^2-1}+\left(\frac{1}{\mu}\right)^2\frac{1}{\sqrt{N^2-1}}+\sqrt{\left(\frac{1}{\mu}\right)^4\left(\sqrt{N^2-1}+\frac{1}{\sqrt{N^2-1}}\right)^2-4}\right)^2} =$$

$$\Delta t_s \sqrt{1+\left(\frac{N^2}{\mu^2\sqrt{N^2-1}}+\frac{1}{\mu^2}\sqrt{\frac{N^4}{N^2-1}-4\mu^4}\right)^2} =$$

$$\Delta t_s \sqrt{1+\left(\frac{N^2+\sqrt{N^4-4\mu^4\left(N^2-1\right)}}{\mu^2\sqrt{N^2-1}}\right)^2}.$$

(23)

In the next step, we can calculate M:

$$M = \frac{\tau_s}{\tau_p} = \frac{\Delta t_s \sqrt{1+\left(\frac{N^2+\sqrt{N^4-4\mu^4\left(N^2-1\right)}}{\mu^2\sqrt{N^2-1}}\right)^2}}{\Delta t_p \cdot N} = \frac{\mu}{N}\sqrt{1+\frac{\left(N^2+\sqrt{N^4-4\mu^4\left(N^2-1\right)}\right)^2}{\mu^4\left(N^2-1\right)}}.$$

(24)

Funding

Hungarian Scientific Research Fund (OTKA) (113083); National Research, Development and Innovation Office (NKFIH) (125808); Hungarian Academy of Sciences (MTA) (János Bolyai Research Scholarship to J. A. Fülöp); Ultrafast physical processes in atoms, molecules, nanostructures and biology structures (EFOP-3.6.2-16-2017-00005).

Acknowledgments

The present scientific contribution is dedicated to the 650th anniversary of the foundation of the University of Pécs, Hungary.

Disclosures

The authors declare that there are no conflicts of interest related to this article.